

Local quantum critical point in the pseudogap Anderson model: finite- T dynamics and ω/T scaling

Matthew T Glossop,* Gareth E Jones, and David E Logan†

Oxford University, Physical and Theoretical Chemistry Laboratory, South Parks Road, Oxford OX1 3QZ, UK.

(Dated: November 22, 2018)

The pseudogap Anderson impurity model is a paradigm for locally critical quantum phase transitions. Within the framework of the local moment approach we study its finite- T dynamics, as embodied in the single-particle spectrum, in the vicinity of the symmetric quantum critical point (QCP) separating generalized Fermi-liquid (Kondo screened) and local moment phases. The scaling spectra in both phases, and at the QCP itself, are obtained analytically. A key result is that pure ω/T -scaling obtains at the QCP, where the Kondo resonance has just collapsed. The connection between the scaling spectra in either phase and that at the QCP is explored in detail.

PACS numbers: 75.20.Hr, 71.10.Hf, 71.27.+a

I. INTRODUCTION

Proximity to a magnetic quantum critical point is one mechanism for non-Fermi liquid behaviour in heavy fermion metals, a topic of great current interest^{1,2}. Experimentally, the temperature below which certain heavy fermion materials become antiferromagnetically ordered can be tuned to $T = 0$ either chemically by doping (e.g. CeCu_{6-x}M_x with M = Au or Ag^{3,4,5}) or through applied pressure (e.g. CeIn₃⁶) or a magnetic field (e.g. YbRh₂Si₂⁷). The transition point then becomes a quantum critical point and leads to non-Fermi liquid behaviour extending over large regions of the phase diagram.

An example that has received much attention is CeCu_{6-x}Au_x^{3,8,9}. For $x < x_c \simeq 0.1$ it is a paramagnet with properties consistent with a highly renormalized Landau Fermi liquid. The localized magnetic moments provided by the Ce atoms, manifest as a Curie-Weiss law at high temperatures, are screened by conduction electrons at low temperatures in a lattice analogue of the familiar Kondo effect for magnetic impurities in metals. For $x > x_c$ by contrast, coupling between local moments wins out and the ground state has antiferromagnetic long-ranged order.

The observed non-Fermi liquid behaviour of CeCu_{5.9}Au_{0.1}^{8,9}, probed by neutron scattering experiments, cannot however be understood in terms of the standard Hertz-Millis mean-field description of a magnetic quantum phase transition based on long wavelength fluctuations of the order parameter^{10,11,12} — the spin dynamics are found to display fractional exponents throughout the Brillouin zone, and satisfy pure ω/T -scaling. This suggests the emergence at the QCP of local moments that are temporally critical, and that temperature is the only energy scale in the problem, cutting off critical quantum fluctuations after a correlation time on the order of $\hbar/k_B T$.

An alternative picture, where critical *local* fluctuations coexist with spatially extended ones, has recently been proposed to explain the above results. Si *et al*¹³ have

shown that such a local quantum critical point arises in the Kondo lattice model through competition between the Kondo exchange coupling — describing the interaction of conduction electron spin and local moment at each lattice site — and the RKKY interaction, which characterizes the coupling between local moments at different lattice sites. At this local QCP the lattice system reaches its magnetic ordering transition at precisely the same point that the Kondo screening becomes critical. Thus the Kondo lattice model, and the self-consistent Bose-Fermi Kondo model to which it reduces with an extended dynamical mean-field theory treatment, are the focus of much current theoretical research^{13,14,15,16,17,18}.

However, significant progress in understanding local QCPs has followed from the study of a simpler problem: the pseudogap Anderson [Kondo] impurity model (PAIM), which serves as a paradigm for locally critical quantum phase transitions, and is the focus of this work. Proposed over a decade ago by Withoff and Fradkin¹⁹, the model represents a generalization of the familiar Anderson [Kondo] impurity model (AIM)²⁰ describing a single magnetic impurity embedded in a non-interacting metallic host (for reviews see Ref. 21,22), and itself enjoying a resurgence of interest in the context of quantum dots and STM experiments^{23,24}.

In the PAIM the fermionic host is described by a power-law density of states vanishing at the Fermi level: $\rho(\omega) \propto |\omega|^r$ with $r > 0$ ($r = 0$ recovers the case of a metallic host). Many specific examples of pseudogap systems *per se* have also been proposed, including various zero-gap semiconductors²⁵, one-dimensional interacting systems²⁶, and the Zn- and Li-doped cuprates^{27,28}. And the possibility that pseudogap physics might be realized in a quantum dot system has also recently been suggested²⁹. The essential physics of the PAIM is by now well understood via a number of techniques, e.g. perturbative scaling^{19,30,31}, numerical renormalization group^{28,32,33,34,35,36}, perturbative renormalization group³⁷, local moment approach^{35,38,39,40}, large- N methods^{19,27,41,42}, non-crossing approximation⁴³ and bare perturbation theory in the interaction strength U ⁴⁴. In contrast to the regular metallic AIM, which exhibits

Fermi liquid physics and a Kondo effect for all U [or J in its Kondo model limit], the PAIM displays in general critical local moment fluctuations and a destruction of the Kondo effect at a finite critical U_c [or J_c]. The quantum critical point, with spin correlations that are critical in time yet spatially local, separates a Fermi liquid Kondo-screened phase ($U < U_c$) from a local moment phase with the characteristics of a free spin-1/2. The key features of the model are summarized in §2.

In an effort to understand better the physics of critical local moment fluctuations, the most recent work on pseudogap impurity models has naturally focused on the QCP itself^{27,36,37,39}, which has been established as a non-Fermi liquid interacting fixed point for $r < 1$ (the upper critical dimension of the problem). For example, Ingersent and Si³⁶ have recently shown that for $r < 1$ the dynamical spin susceptibility at the critical point exhibits ω/T -scaling with a fractional exponent, which features closely parallel those of the local QCP of the Kondo lattice. A very recent perturbative renormalization group study³⁷ has developed critical theories for the transition, confirming that, for $0 < r < 1$ the transition is described by an interacting field theory with universal local moment fluctuations and hyperscaling, including ω/T -scaling in the dynamics.

In this paper, using the local moment approach (LMA), we develop an analytical description of finite- T dynamics in the vicinity of the QCP, as embodied in the local single-particle spectrum $D(\omega)$. Developed originally to describe metallic AIMs at $T = 0$ ^{45,46,47}, and subsequently extended to handle finite temperatures⁴⁸ and magnetic fields^{49,50}, the LMA has also been applied to the PAIM^{38,39,40} leading to a number of new predictions that have since been confirmed by NRG calculations³⁵. We also add that the approach can encompass lattice-based models within dynamical mean-field theory, e.g. the periodic Anderson model appropriate to the paramagnetic metallic phase of heavy fermion materials^{51,52,53}.

The paper is organized as follows. After the necessary background, section 2, we present in section 3 a number of exact results for the scaling spectra in both phases of the model, and at the QCP itself, using general scaling arguments. In section 4 a brief description is given of the finite- T local moment approach to the problem, along with a numerical demonstration of scaling of the single-particle dynamics. An analytical description, arising within the LMA, of the finite- T scaling spectrum for both phases and at the QCP is given in section 5, and is found to be in excellent agreement with the numerics. The connection between the scaling spectra in either phase and that at the QCP itself is explored fully, ω/T -scaling of $D(\omega)$ at the QCP being one key result. The paper concludes with a brief summary.

II. BACKGROUND

The Hamiltonian for an AIM is given in standard notation by

$$\hat{H} = \sum_{\mathbf{k},\sigma} \epsilon_{\mathbf{k}} \hat{n}_{\mathbf{k}\sigma} + \sum_{\sigma} (\epsilon_i + \frac{U}{2} \hat{n}_{i-\sigma}) \hat{n}_{i\sigma} + \sum_{\mathbf{k},\sigma} V_{i\mathbf{k}} (c_{i\sigma}^{\dagger} c_{\mathbf{k}\sigma} + \text{h.c.}) \quad (2.1)$$

where the first term describes the non-interacting host with dispersion $\epsilon_{\mathbf{k}}$ and density of states $\rho(\omega) = \sum_{\mathbf{k}} \delta(\omega - \epsilon_{\mathbf{k}})$ (with $\omega = 0$ the Fermi level). The second term describes the correlated impurity, with energy ϵ_i and local interaction U , and the third the host-impurity coupling (via $V_{i\mathbf{k}} \equiv V$).

For a conventional metallic host the Fermi level density of states $\rho(0) \neq 0$, and low-energy states are always available for screening. In consequence the impurity spin is quenched and the system a Fermi liquid for all U (see e.g.²¹). For the pseudogap AIM (PAIM) by contrast the host density of states is soft at the Fermi level, $\rho(\omega) \propto |\omega|^r$ ($r > 0$)¹⁹. Due to the depletion of host states around the Fermi level, the PAIM exhibits a quantum phase transition^{19,27,28,30,31,32,33,34,35,36,38,39,40,41,42} at a critical $U = U_c(r)$, the quantum critical point (QCP) separating a degenerate local moment (LM) phase for $U > U_c$ from a ‘strong coupling’ or generalized Fermi liquid (GFL) phase, $U < U_c$, in which the impurity spin is locally quenched and a Kondo effect manifest. As $r \rightarrow 0$ the critical $U_c(r)$ diverges ($\sim 1/r$)^{33,34,35,38,39,40}, symptomatic of the absence of a transition for the conventional metallic AIM corresponding to $r = 0$, and whose behaviour is recovered smoothly in the $r \rightarrow 0$ limit^{38,39,40}. In the present paper we focus on the so-called symmetric QCP that arises in both the particle-hole (p-h) symmetric and asymmetric PAIM³⁴. To that end we consider explicitly the p-h symmetric model, with $\epsilon_i = -\frac{1}{2}U$ (and impurity charge $n_i = \sum_{\sigma} \langle \hat{n}_{i\sigma} \rangle = 1$). In this case the QCP is known to separate GFL/LM phases for all $0 < r < \frac{1}{2}$ ^{33,34,35,38,39} (for $r > \frac{1}{2}$ the LM phase alone arises for any $U > 0$).

Our focus here is on single-particle dynamics at finite- T , embodied in the (retarded) impurity Green function $G(\omega, T)$ ($\leftrightarrow -i\theta(t)\langle\{c_{i\sigma}(t), c_{i\sigma}^{\dagger}\}\rangle$), with $D(\omega, T) = -\frac{1}{\pi}\text{Im}G(\omega, T)$ the single-particle spectrum. $G(\omega, T)$ may be expressed as

$$G(\omega, T) = [\omega^+ - \Delta(\omega) - \Sigma(\omega, T)]^{-1} \quad (2.2)$$

with $\omega^+ = \omega + i0^+$ and $\Sigma(\omega, T) = \Sigma^R(\omega, T) - i\Sigma^I(\omega, T)$ the conventional single self-energy (defined to exclude the trivial Hartree term which precisely cancels $\epsilon_i = -\frac{1}{2}U$), such that $\Sigma(\omega, T) = -[\Sigma(-\omega, T)]^*$ by p-h symmetry. All effects of host-impurity coupling at the one-electron level are embodied in the hybridization function $\Delta(\omega) = \sum_{\mathbf{k}} V_{i\mathbf{k}}^2 [\omega^+ - \epsilon_{\mathbf{k}}]^{-1} = \Delta_R(\omega) - i\Delta_I(\omega)$. For the PAIM considered here, $\Delta_I(\omega) = \pi V^2 \rho(\omega)$ is given explicitly by $\Delta_I(\omega) = \Delta_0 (|\omega|/\Delta_0)^r \theta(D - |\omega|)$ with Δ_0 the hybridization strength, D the bandwidth and $\theta(x)$ the unit step

function. Throughout the paper we take $\Delta_0 \equiv 1$ as the energy unit, i.e.

$$\Delta_I(\omega) = |\omega|^r \theta(D - |\omega|). \quad (2.3)$$

The real part of the hybridization function follows simply from Hilbert transformation,

$$\Delta_R(\omega) = -\text{sgn}(\omega) \left[\beta(r) \Delta_I(\omega) + \mathcal{O}\left(\frac{|\omega|}{D}\right) \right] \quad (2.4)$$

with $\beta(r) = \tan(\frac{\pi r}{2})$. That this form for the hybridization is simplified is of course irrelevant to the low-energy scaling behaviour of the problem, in the same way that the usual ‘flat band’ caricature of the metallic host is immaterial to the intrinsic Kondo physics of the metallic AIM²¹.

We now summarize key characteristics of the problem at $T = 0$ ^{19,27,28,30,31,32,33,34,35,36,38,39,40,41,42} that are required in the remainder of the paper, including the essential manner in which the underlying transition is directly apparent in single-particle dynamics.

A. GFL phase

For *all* $U < U_c(r)$ in the GFL phase ($0 < r < \frac{1}{2}$), the leading low- ω behaviour of $D(\omega, 0)$ is entirely unrenormalized from the non-interacting limit and given by

$$\pi D(\omega, 0) \stackrel{|\omega| \rightarrow 0}{\sim} \cos^2\left(\frac{\pi r}{2}\right) |\omega|^{-r}. \quad (2.5)$$

This is an exact result⁴⁴. It arises because $\Sigma^{R/I}(\omega, 0)$ vanish as $\omega \rightarrow 0$ more rapidly than the hybridization ($\propto |\omega|^r$), reflecting in physical terms the perturbative continuity to the non-interacting limit that in essence defines a Fermi liquid. The leading low- ω behaviour of $\Sigma^R(\omega, 0)$ is in fact given by

$$\Sigma^R(\omega, 0) \stackrel{\omega \rightarrow 0}{\sim} -\left(\frac{1}{Z} - 1\right) \omega \quad (2.6)$$

as one would cursorily expect from p-h symmetry ($\Sigma^R(\omega, 0) = -\Sigma^R(-\omega, 0)$); with the quasiparticle weight (or mass renormalization) Z defined as usual by $Z = [1 - (\partial \Sigma^R(\omega, 0) / \partial \omega)_{\omega=0}]^{-1}$. By virtue of equation (2.5) the most revealing exposé of GFL dynamics at $T = 0$ lies in the modified spectral function $\mathcal{F}(\omega, 0)$ ^{35,38,39,40}, defined generally by

$$\mathcal{F}(\omega, T) = \pi \sec^2\left(\frac{\pi r}{2}\right) |\omega|^r D(\omega, T) \quad (2.7)$$

such that $\mathcal{F}(0, 0) = 1$ (i.e. the $T = 0$ modified spectrum is ‘pinned’ at the Fermi level, a result that reduces to the trivial dictates of the Friedel sum rule for the $r = 0$ metallic AIM²¹).

The Kondo resonance is directly apparent in $\mathcal{F}(\omega, 0)$ ^{35,38,39,40} — see e.g. figure 16 of Ref. 38, and figure 3 below. Indeed on visual inspection it is barely

distinguishable from its $r = 0$ metallic counterpart, to which it reduces for $r = 0$. The resonance is naturally characterised by a low-energy Kondo scale ω_K , usually defined in practice by the width of the resonance³⁵. Most importantly, as $U \rightarrow U_c^-$ and the GFL \rightarrow LM transition is approached, the Kondo scale becomes arbitrarily small (vanishing at the QCP itself, where the Kondo resonance collapses). For $r \ll 1$ it is well-established from previous LMA work and NRG calculations^{35,38,39,40} that ω_K vanishes according to $\omega_K \propto (1 - U/U_c(r))^{\frac{1}{r}}$.

In consequence, in the vicinity of the transition, $\mathcal{F}(\omega, 0)$ exhibits *universal scaling behaviour* in terms of ω/ω_K ^{35,38}. It is of course in this scaling behaviour that the underlying quantum phase transition is directly manifest^{39,40}.

B. LM phase

The local moment phase is more subtle than naive expectation might suggest. Here it is known, originally from NRG calculations³³, that the leading low- ω behaviour of $D(\omega, 0)$ is

$$D(\omega, 0) \stackrel{|\omega| \rightarrow 0}{\sim} c |\omega|^r \quad (2.8)$$

(with $\text{Re}G(\omega, 0) \sim -\text{sgn}(\omega) \pi \beta(r) D(\omega, 0)$ following directly from Hilbert transformation). From this alone, simply by inverting equation (2.2), the leading low- ω behaviour of the single self-energy $\Sigma^R(\omega, 0)$ is given by

$$\Sigma^R(\omega, 0) \stackrel{|\omega| \rightarrow 0}{\sim} \text{sgn}(\omega) \sin(\pi r) \frac{1}{2\pi D(\omega, 0)} \propto |\omega|^{-r} \quad (2.9)$$

(and likewise $\Sigma^I(\omega, 0) \propto \Sigma^R(\omega, 0)$). This divergent low- ω behaviour is radically different from the simple analyticity of its counterpart equation (2.6) in the GFL phase, and illustrates the basic difficulty: the need to capture within a common framework such distinct behaviour in the GFL and LM phases, indicative of the underlying phase transition and as such requiring an inherently non-perturbative description. We do not know of any theoretical approach based on the conventional single self-energy that can handle this issue.

There is however nothing sacrosanct in direct use of the single self-energy, which is merely defined by the Dyson equation implicit in equation (2.2). Indeed for the doubly-degenerate LM phase, a physically far more natural approach would be in terms of a two-self-energy description (as immediately obvious by consideration e.g. of the atomic limit — the ‘extreme’ LM case). Here the rotationally invariant $G(\omega, T)$ is expressed as

$$G(\omega, T) = \frac{1}{2} [G_{\uparrow}(\omega, T) + G_{\downarrow}(\omega, T)] \quad (2.10)$$

with the $G_{\sigma}(\omega, T)$ given by

$$G_{\sigma}(\omega, T) = [\omega^+ - \Delta(\omega) - \tilde{\Sigma}_{\sigma}(\omega, T)]^{-1} \quad (2.11)$$

in terms of spin-dependent self-energies $\tilde{\Sigma}_\sigma(\omega, T)$ ($= \tilde{\Sigma}_\sigma^R(\omega, T) - i\tilde{\Sigma}_\sigma^I(\omega, T)$); satisfying

$$\tilde{\Sigma}_\sigma(\omega, T) = -[\tilde{\Sigma}_{-\sigma}(-\omega, T)]^* \quad (2.12)$$

for the p-h symmetric case considered. It is precisely this two-self-energy framework that underlies the LMA^{38,39,40,45,46,47,48,49,50} (with the single self-energy obtained if desired as a byproduct, following simply from direct comparison of equations (2.10, 11) with equation (2.2)); requisite details will be given in section 4. The LM phase is then characterised by *non-vanishing*, spin-dependent ‘renormalized levels’ $\tilde{\Sigma}_\sigma^R(0, 0) = -\tilde{\Sigma}_{-\sigma}^R(0, 0)$ (so called because they correspond to $\tilde{\epsilon}_{i\sigma} = \epsilon_i + \tilde{\Sigma}_\sigma^R(0, 0)$ if the Hartree contribution is explicitly retained in the $\tilde{\Sigma}_\sigma^R(\omega, 0)$). From this, using equations (2.10,11), the low- ω behaviour embodied in equation (2.8) (and hence equation (2.9) for the single self-energy) *follows directly*, namely

$$\pi D(\omega, 0) \stackrel{|\omega| \rightarrow 0}{\propto} |\omega|^r / [\tilde{\Sigma}_\sigma^R(0, 0)]^2 \quad (2.13)$$

(assuming merely that $\tilde{\Sigma}_\sigma^I(\omega, 0)$ vanishes no more rapidly than the hybridization $\propto |\omega|^r$). As $U \rightarrow U_c+$ and the LM \rightarrow GFL transition is approached, the renormalized level $\tilde{\Sigma}_\sigma^R(0, 0) \rightarrow 0$ ^{39,40}; and $\tilde{\Sigma}_\sigma^R(0, 0) = 0$ remains throughout the (‘symmetry unbroken’) GFL phase $U < U_c$ ^{38,39,40}, such that the characteristic low- ω spectral behaviour equation (2.5) is likewise correctly recovered.

The underlying two-self-energy description is thus capable of handling both phases simultaneously, and hence the transition between them. Further, since the renormalized level $|\tilde{\Sigma}_\sigma^R(0, 0)|$ vanishes as the LM \rightarrow GFL transition is approached, it naturally generates a low-energy scale ω_L characteristic of the LM phase (defined precisely in section 5.2); in terms of which LM phase dynamics in the vicinity of the transition have recently been shown^{39,40} to exhibit universal scaling. This behaviour is of course the counterpart of the Kondo scale ω_K and associated spectral scaling in the GFL phase, but now for the LM phase on the other side of the underlying quantum phase transition.

III. SCALING: GENERAL CONSIDERATIONS

Close to and on either side of the quantum phase transition, the problem is thus characterised by a single low-energy scale, denoted generically by ω_* (the Kondo scale for the GFL phase; ω_L for the LM phase). Given this, and without recourse to any particular theory, we now show that general scaling arguments may be used to obtain a number of exact results for the finite- T scaling spectra, in both the GFL and LM phases *and at the QCP itself* (where $\omega_* = 0$ identically). These are important in themselves, and in addition provide stringent dictates that should be satisfied by any approximate theoretical approach to the problem.

We consider first the case of $T = 0$, for which general scaling arguments made by us in⁴⁰ serve as a starting point. In the following we denote the spectrum by $D(U; \omega)$, with the U -dependence temporarily explicit. As the transition is approached, $u = |1 - U/U_c(r)| \rightarrow 0$, the low-energy scale ω_* vanishes, as

$$\omega_* = u^a \quad (3.1)$$

with exponent a . $D(U; \omega)$ can now be expressed generally in the scaling form $\pi D(U; \omega) = u^{-ab} \Psi_\alpha(\omega/u^a)$ in terms of two exponents a and b (and with $\alpha = \text{GFL or LM}$ denoting the appropriate phase), i.e. as

$$\pi \omega_*^b D(U; \omega) = \Psi_\alpha(\omega/\omega_*) \quad (3.2)$$

with the exponent a eliminated and the ω -dependence encoded solely in $\omega/\omega_* = \tilde{\omega}$. Equation (3.2) simply embodies the universal scaling behaviour of the $T = 0$ single-particle spectrum close to the QPT. Using it, three results follow:

(i) That the exponent $b = r$ for the GFL phase (and for all r where the GFL phase arises). This follows directly from equation (3.2) using the fact that the leading $\omega \rightarrow 0$ behaviour of $D(U; \omega)$ throughout the GFL phase is given exactly by equation (2.5), together with the fact that $\Psi_\alpha(x)$ is universal; i.e.

$$\pi \omega_*^r D(U; \omega) = \Psi_\alpha(\omega/\omega_*). \quad (3.3)$$

(ii) Now consider the approach to the QCP, $\omega_* \rightarrow 0$ and hence $\omega/\omega_* \rightarrow \infty$. Since the QCP itself must be ‘scale free’ (independent of ω_*), equation (3.3) implies

$$\Psi_\alpha(\omega/\omega_*) \stackrel{|\omega/\omega_* \rightarrow \infty}{\sim} C(r) (|\omega/\omega_*|)^{-r} \quad (3.4)$$

with $C(r)$ a constant (naturally r -dependent). From equations (3.3,4) it follows directly that precisely at the QCP ($\omega_* = 0$),

$$\pi D(U_c; \omega) = C(r) |\omega|^{-r} \quad (3.5)$$

which gives explicitly the ω -dependence of the ($T = 0$) QCP spectrum.

(iii) Assuming naturally that the QCP behaviour is independent of the phase from which it is approached, equation (3.4) applies also to the LM phase. From equations (3.2) and (3.4) it follows that the exponent $b = r$ for the LM phase as well (as one might expect physically).

The above behaviour is indeed as found in practice from the LMA at $T = 0$ ^{38,39,40}, with the scaling for equation (3.3) also confirmed by NRG calculations³⁵. But the important point here is that these results are general, independent of approximations (be they analytical or numerical), and as such holding across the entire r -range for which the symmetric QCP exists, i.e. $0 < r < \frac{1}{2}$ ³⁴. We add moreover that while the argument above for $b = r$ leading to equation (3.3) is particular to the symmetric PAIM considered explicitly here, recent LMA results for the asymmetric PAIM for $0 < r < 1$ ⁴⁰, and NRG

results²⁸ for the asymmetric pseudogap Kondo model for $\frac{1}{2} < r < 1$, are also consistent with the exponent $b = r$. The QCP behaviour equation (3.5) then follows directly, and the LMA/NRG results of Ref. 28,40 are likewise consistent with it.

The arguments above⁴⁰ can now be extended to finite temperature. The scaling spectra may again be cast generally in the form $\pi D(U; \omega, T) = u^{-ar} \Psi_\alpha(\omega/u^a, T/u^a)$, i.e. as

$$\pi \omega_*^r D(U; \omega, T) = \Psi_\alpha(\omega/\omega_*, T/\omega_*) \quad (3.6)$$

expressing the fact that $\omega_*^r D(U; \omega, T)$ is a universal function of $\tilde{\omega} = \omega/\omega_*$ and $\tilde{T} = T/\omega_*$. From this follow three results, new to our knowledge:-

(i) Consider first the approach to the QCP at finite- T , i.e. $\tilde{\omega} \rightarrow \infty$ and $\tilde{T} \rightarrow \infty$ such that $\tilde{\omega}/\tilde{T} = \omega/T$ is fixed. Again, since the QCP must be scale free, $\Psi_\alpha(\tilde{\omega} \rightarrow \infty, \tilde{T} \rightarrow \infty)$ must be of form $\tilde{T}^p S(\omega/T)$ with the exponent $p = -r$ from equation (3.6), i.e.

$$\Psi_\alpha(\tilde{\omega}, \tilde{T}) \sim \tilde{T}^{-r} S(\omega/T). \quad (3.7)$$

(ii) From equations (3.6,7) it follows directly that precisely at the QCP ($\omega_* = 0$):

$$\pi T^r D(U_c; \omega, T) = S(\omega/T) \quad (3.8)$$

i.e. $T^r D(U_c; \omega, T)$ exhibits *pure* ω/T -scaling.

(iii) The large- x behaviour of $S(x)$ — and hence the ‘tail’ behaviour of the QCP scaling spectrum $S(\omega/T)$ — may be deduced on the natural assumption that the limits $\omega_* \rightarrow 0$ and $T \rightarrow 0$ commute; i.e. that the $T = 0$ QCP spectrum may either be obtained at $T = 0$ from the limit $\omega_* \rightarrow 0$ (as in equation (3.5)), or from the $T \rightarrow 0$ limit of the finite- T QCP scaling spectrum equation (3.8) (in which $\omega_* \rightarrow 0$ has been taken first). With this, comparison of equations (3.5,8) yields the desired result

$$S(\omega/T) \stackrel{|\omega|/T \rightarrow \infty}{\sim} C(r) (|\omega|/T)^{-r}. \quad (3.9)$$

The behaviour embodied in equations (3.7–9) follows on general grounds. In particular, the ω/T -scaling of the QCP scaling spectrum is a key conclusion. Neither is such scaling specific to single-particle dynamics. For the dynamical local magnetic susceptibility, recent NRG calculations³⁶ are consistent with ω/T -scaling at the QCP (for $0 < r < 1$), as supported further by approximate analytic results for small r based on a procedure analogous to the standard ϵ -expansion. The preceding arguments do *not* of course determine the functional form of the scaling spectra embodied in the $\Psi_\alpha(\tilde{\omega}, \tilde{T})$ and $S(\omega/T)$, save for their asymptotic form equations (3.4,9): for that a ‘real’ (inevitably approximate) theory is required, as considered in the following sections; and from which the general results above should of course be recovered. We note in passing that the arguments above also encompass the role of a local magnetic field, $h = \frac{1}{2} g \mu_B H_{\text{loc}}$ (with $\tilde{h} = h/\omega_*$ in the following): replacing T by h in equations (3.6-9) gives the appropriate

scaling behaviour in terms of $\tilde{\omega}$ and \tilde{h} (for $T = 0$). At the QCP in particular $h^r D(U_c; \omega, h)$ exhibits *pure* ω/h -scaling,

$$\pi h^r D(U_c; \omega, h) = S'(\omega/h) \quad (3.10)$$

with the large- $|\omega|/h$ ‘tail’ behaviour $S'(\omega/h) \sim C(r) (|\omega|/h)^{-r}$.

A. The low-energy scale

Before proceeding we return briefly to an obvious issue: the physical nature of the low-energy scale ω_* . In the GFL phase for example, how is it related to the quasiparticle weight $Z = [1 - (\partial \Sigma^R(\omega; 0)/\partial \omega)_{\omega=0}]^{-1}$, which we likewise expect to vanish as $U \rightarrow U_c(r)$ —,

$$Z \sim u^{a_1} \quad (3.11)$$

with exponent a_1 ? That question may be answered most simply (albeit partially here) by considering the limiting low-frequency ‘quasiparticle form’ for the impurity Green function, whose behaviour reflects the adiabatic continuity to the non-interacting limit that is intrinsic to the GFL phase. This follows from the low- ω expansion of the single self-energy, $\Sigma(\omega; 0) \sim -(\frac{1}{Z} - 1)\omega$ (with the imaginary part neglected as usual²¹); using which with equations (2.2–4) yields the quasiparticle behaviour

$$\pi D(U; \omega) \sim \frac{|\omega|^r}{(\frac{\omega}{Z} + \text{sgn}(\omega)\beta(r)|\omega|^r)^2 + |\omega|^{2r}} \quad (3.12)$$

which itself must be expressible in the scaling form equation (3.3). This in turn implies that ω_* and Z are related by

$$\omega_* = [k_1 Z]^{1/(1-r)} \quad (3.13)$$

(with k_1 an arbitrary constant up to which low-energy scales are defined), such that equation (3.12) reduces to the required form

$$\pi \omega_*^r D(U; \omega) \sim \frac{|\tilde{\omega}|^r}{(k_1 |\tilde{\omega}| + \text{sgn}(\omega)\beta(r)|\tilde{\omega}|^r)^2 + |\tilde{\omega}|^{2r}} \quad (3.14)$$

with $\tilde{\omega} = \omega/\omega_*$. For the GFL phase the ω_* ($\equiv \omega_K$) scale and the quasiparticle weight Z are thus related by equation (3.13) (and hence the exponents a (equation (3.1)) and a_1 (equation (3.11)) by $a_1 = a(1-r)$). That behaviour is correctly recovered by the LMA, which in addition shows ω_* to be equivalently the characteristic Kondo spin-flip scale associated with transverse spin excitations; see section 5.1 below.

In contrast to the GFL phase where the leading low- ω spectral behaviour is $D(U; \omega) \propto |\omega|^{-r}$ as above, the corresponding behaviour for the LM phase is given by $\pi D(U; \omega) \propto |\omega|^r / [\Sigma_\sigma^R(0; 0)]^2$ (equation (2.13)) in terms

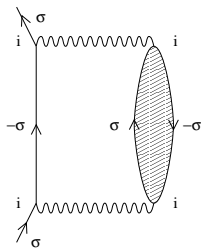


FIG. 1: Standard LMA diagram for the dynamical contribution Σ_σ to the self-energies.

of the ‘renormalized level’ $\tilde{\Sigma}_\sigma^R(0;0)$, which is non-zero in the LM phase and vanishes as $U \rightarrow U_c(r)^+$ ^{39,40}; i.e.

$$|\tilde{\Sigma}_\sigma^R(0;0)| \sim u^{a_2} \quad (3.15)$$

with exponent a_2 . Since equation (2.13) must be expressible in the scaling form equation (3.3) it follows that ω_* ($\equiv \omega_L$) in the LM phase is related simply to the renormalized level by

$$\omega_* = [k_2 |\tilde{\Sigma}_\sigma^R(0;0)|]^\frac{1}{a_2} \quad (3.16)$$

(and hence the exponents a and a_2 by $a_2 = ar$). We emphasize again that the exponents obtained above are exact, valid for all $0 < r < \frac{1}{2}$.

After the above general considerations we now consider the finite-temperature scaling properties of the PAIM within the local moment approach.

IV. LOCAL MOMENT APPROACH: FINITE T

Regardless of the phase considered the LMA uses the two-self energy description embodied in equations (2.10,11), with the self-energies separated for convenience as

$$\tilde{\Sigma}_\sigma(\omega^+, T) = -\frac{\sigma}{2}U|\mu| + \Sigma_\sigma(\omega^+, T) \quad (4.1)$$

into a purely static Fock piece with local moment $|\mu|$ (that is retained alone at mean-field level); and an all important dynamical contribution $\Sigma_\sigma(\omega^+, T)$ containing the spin-flip physics that dominates at low-energies. The $G_\sigma(\omega, T)$ (equation (2.11)) may be recast equivalently as

$$G_\sigma(\omega, T) = [\mathcal{G}_\sigma(\omega)^{-1} - \Sigma_\sigma(\omega^+, T)]^{-1} \quad (4.2)$$

in terms of the mean-field (MF) propagators

$$\mathcal{G}_\sigma(\omega) = [\omega^+ + \frac{\sigma}{2}U|\mu| - \Delta(\omega)]^{-1} \quad (4.3)$$

and with $\Sigma_\sigma \equiv \Sigma_\sigma[\{\mathcal{G}_\sigma\}]$ a functional of the $\{\mathcal{G}_\sigma(\omega)\}$.

The standard LMA diagrammatic approximation for the t -ordered two-self-energies is depicted in figure 1. For full details, including their physical interpretation, the

reader is referred to^{38,45,47}. In retarded form at finite temperature, $\Sigma_\uparrow(\omega)$ is given by⁴⁸

$$\begin{aligned} \Sigma_\uparrow(\omega^+, T) &= U^2 \int_{-\infty}^{\infty} \frac{d\omega_1}{\pi} \int_{-\infty}^{\infty} d\omega_2 \chi^{+-}(\omega_1, T) \\ &\times \frac{D_\downarrow^0(\omega_2)}{\omega + \omega_1 - \omega_2 + i\eta} g(\omega_1; \omega_2) \end{aligned} \quad (4.4)$$

where $D_\sigma^0(\omega) = -\frac{1}{\pi}\text{Im}\mathcal{G}_\sigma(\omega)$ is the MF spectral density; and $g(\omega_1; \omega_2) = \theta(-\omega_1) [1 - f(\omega_2; T)] + \theta(\omega_1)f(\omega_2; T)$ with $f(\omega; T) = [1 + \exp(\omega/T)]^{-1}$ the Fermi function. $\chi^{+-}(\omega, T) \equiv \text{Im}\Pi^{+-}(\omega, T)$ is the spectrum of transverse spin excitations, with $\Pi^{+-}(\omega, T)$ the finite- T polarization propagator, calculated via an RPA-like p-h ladder sum⁴⁸. $\Sigma_\downarrow(\omega) = -[\Sigma_\uparrow(-\omega)]^*$ follows trivially by particle-hole symmetry; we thus choose to work with $\Sigma_\uparrow(\omega)$.

The T -dependence of the $\chi^{+-}(\omega, T)$, and also of the local moment $|\mu| = |\mu(T)|$ entering the MF propagators (equation(4.3)) and self-energies (equation (4.1)), is found to be insignificantly small, provided we remain uninterested in temperatures on the order of the non-universal energy scales in the problem. This is precisely as for the $r = 0$ case⁴⁸ and we thus work with $\chi^{+-}(\omega, T) \simeq \chi^{+-}(\omega, T = 0) \equiv \text{Im}\Pi^{+-}(\omega)$ and local moment $|\mu(0)| \equiv |\mu|$. The remaining T -dependence, describing the universal scaling regime, is controlled solely by $g(\omega_1; \omega_2)$ entering equation (4.4).

In describing the GFL phase within the LMA, the key concept is that of symmetry restoration (SR)^{38,40,45,47}: self-consistent restoration of the symmetry broken at pure MF level. In mathematical terms this is encoded simply in $\tilde{\Sigma}_\uparrow(0^+, T = 0) = \tilde{\Sigma}_\downarrow(0^+, T = 0)$ and hence, via particle-hole symmetry,

$$\left[\tilde{\Sigma}_\uparrow(0^+; T = 0) \equiv \right] \Sigma_\uparrow(0) - \frac{1}{2}U|\mu| = 0. \quad (4.5)$$

Equation (4.5) guarantees in particular the correct Fermi liquid form $\mathcal{F}(0,0) = 1$ (see equation (2.7)). It is satisfied in practice, for any given $U < U_c$, by varying the local moment $|\mu|$ entering the MF propagators from the pure MF value $|\mu_0| < |\mu|$ until equation (4.5) — a single condition at the Fermi level $\omega = 0$ — is satisfied. In so doing a low-energy scale is introduced into the problem through a strong resonance in $\text{Im}\Pi^{+-}(\omega)$ centred on $\omega = \omega_m \equiv \omega_m(r)$. This is the Kondo or spin-flip scale $\omega_m \propto \omega_K$ and sets the timescale for symmetry restoration, $\tau \sim \hbar/\omega_m$ ^{38,40,45,47}.

In the LM phase, by contrast, it is not possible to satisfy the symmetry restoration condition equation (4.5) and $|\mu| = |\mu_0|$ ^{38,40}: $\text{Im}\Pi^{+-}(\omega)$ then correctly contains a delta-function contribution at $\omega = 0$, reflecting physically the zero-energy cost for spin-flips in the doubly-degenerate LM phase. The ‘renormalized levels’ (see section 2.2) $\{\tilde{\Sigma}_\sigma(0,0)\}$ are here found to be non-zero and sign-definite.

The GFL/LM phase boundary, i.e. $U_c \equiv U_c(r)$, may then be accessed either as the limit of solutions to equation (4.5), where $\omega_m \rightarrow 0$; or, coming from the LM side,

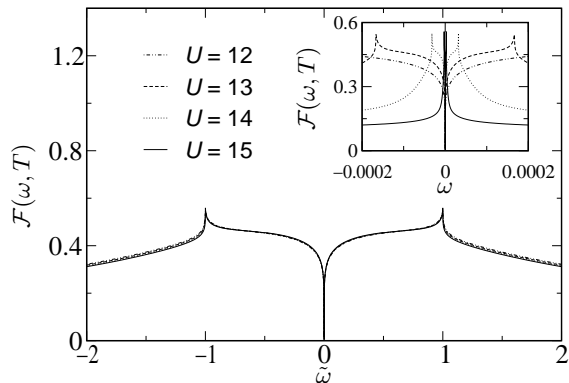


FIG. 2: GFL phase scaling spectrum $\mathcal{F}(\omega, T) = \pi \text{sec}^2(\frac{\pi}{2}r)|\omega|^r D(\omega, T)$ versus $\tilde{\omega} = \omega/\omega_m$, for fixed $\tilde{T} = T/\omega_m = 1$ and four values of the interaction strength U approaching $U_c \simeq 16.4$. The inset shows $\mathcal{F}(\omega, T)$ on an absolute scale.

as the limiting U for which the $\{\tilde{\Sigma}_\sigma(0, 0)\}$ vanish. In either case the *same* $U_c(r)$ obtains; and both GFL and LM phases are correctly found to arise for all $0 < r < \frac{1}{2}$, while solely LM states occur for all $r > \frac{1}{2}$ and $U > 0$ ³⁸. For $r \rightarrow 0$ the LMA recovers the exact result that $U_c = 8/\pi r$ which, together with the low- r result $a = 1/r$ (see equation (3.1))³⁸ recovers the exact exponential dependence of the regular $r = 0$ metallic AIM²¹.

The practical strategy for solving the problem at finite- T is likewise straightforward. Once the local moment $|\mu|$ is known from symmetry restoration (for any given r and U), the dynamical self-energy $\Sigma_\uparrow(\omega^+, T)$ follows from equation (4.4). The full self-energy then follows immediately from equation (4.1) and $G(\omega, T)$ in turn via equations (4.2) and (2.10). We now give numerical results obtained in this way for the GFL phase at finite- T .

A. Numerical results: GFL phase scaling

Here we show that the LMA correctly captures scaling of the single-particle spectrum $D(\omega, T)$ as the transition is approached, $U \rightarrow U_c(r)-$. That is, $\omega_m^r D(\omega, T)$ scales in terms of both $\tilde{\omega} = \omega/\omega_m$ and $\tilde{T} = T/\omega_m$, as expressed in equation (3.6); or equivalently that $\mathcal{F}(\omega, T) \equiv F(\tilde{\omega}, \tilde{T})$.

Figure 2 shows the numerically determined spectral function $\mathcal{F}(\omega, T)$ versus $\tilde{\omega} = \omega/\omega_m$ for $r = 0.2$, a fixed temperature $\tilde{T} = T/\omega_m = 1$ and four values of $U < U_c(r)$ as the transition is approached ($U_c \simeq 16.4$). The spectra — very different on an absolute scale as shown in the inset to the figure — indeed clearly collapse to a common scaling form as $U \rightarrow U_c(r)-$ and ω_m becomes arbitrarily small.

This behaviour is not of course particular to the choice $\tilde{T} = 1$, but rather is found to arise for all (finite) \tilde{T} . Figure 3 shows the resultant scaling spectra for a repre-

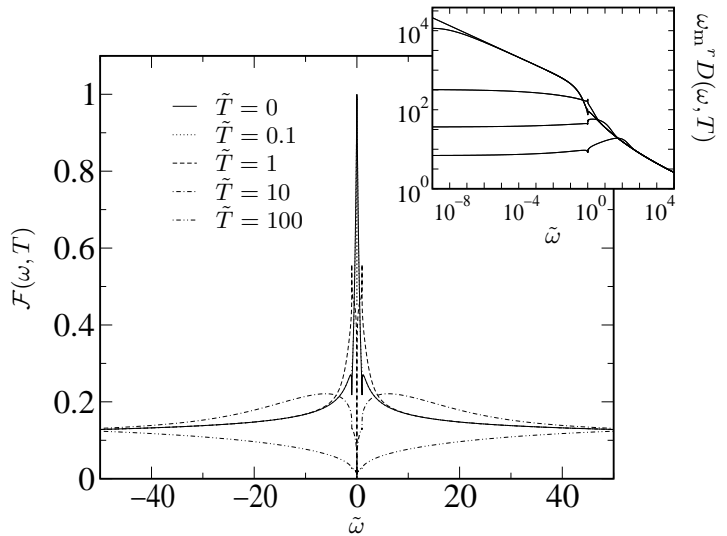


FIG. 3: Numerical results: GFL phase scaling spectrum $\mathcal{F}(\omega, T)$ versus $\tilde{\omega} = \omega/\omega_m$ for a range of $\tilde{T} = T/\omega_m$. The generalized Kondo resonance is thermally destroyed, with the principal effects of temperature arising for $|\tilde{\omega}| \lesssim \tilde{T}$. The inset shows $\omega_m^r D(\omega, T)$ versus $\tilde{\omega}$ on a logarithmic scale for the same \tilde{T} , increasing top to bottom; see text for comments.

sentative range of \tilde{T} , labelled in the figure. For $T = 0$ the GFL phase Kondo resonance is fully present and $\mathcal{F}(\omega = 0, T = 0) = 1$, as discussed in section 3. As temperature is raised through a range on the order of the Kondo scale itself ($\tilde{T} \sim \mathcal{O}(1)$) the Kondo resonance is thermally destroyed. First it is split — reflecting the fact that the Fermi level $D(\omega = 0, T)$ is finite for $T > 0$ (see inset) — and then progressively eroded as \tilde{T} increases. For any given temperature \tilde{T} the principal effect of temperature arises on frequency scales $|\tilde{\omega}| \lesssim \tilde{T}$, such that for $\tilde{\omega} \gg \tilde{T}$ the spectrum is essentially coincident with the $\tilde{T} = 0$ limit. This behaviour is observed clearly in the inset to figure 3 wherein e.g. the $\tilde{T} = 1$ scaling spectrum is coincident with that for $\tilde{T} = 0$ for $|\tilde{\omega}| \gtrsim 10$; and that for $\tilde{T} = 10$ coincides with $\tilde{T} = 0$ for $|\tilde{\omega}| \gtrsim 50$. We also add that the small spectral feature at $\tilde{\omega} \simeq 1$, seen e.g. in the inset to figure 3, is entirely an artefact of the specific RPA form for $\text{Im}\Pi^{\pm-}(\omega)$ that, as discussed in detail in previous work⁴⁶, can be removed entirely with both little effect on the appearance of the spectrum and no effect on any asymptotic results.

V. RESULTS

We now turn to an analytical description of the finite- T scaling spectrum in the strong coupling (= strongly correlated) limit of $U \gg 1$. As in Ref. 39, and in contrast to the results of section 3, this formally restricts discussion to $r \ll 1$, although as demonstrated below such an

analysis does rather well in accounting for the numerical results given in section 4.1 for $r = 0.2$. For this reason we present only analytical results in the remainder of the paper, where we focus in turn on the GFL phase, LM phase and the QCP itself.

A. GFL phase

To obtain the scaling behaviour of $D(\omega)$ we consider finite $\tilde{\omega} = \omega/\omega_m$ in the formal limit $\omega_m \rightarrow 0$, thereby projecting out irrelevant non-universal spectral features (e.g. the Hubbard bands at $\omega \sim \pm U/2$). Using equations (2.10,11) the scaling spectrum $\omega_m^r D(\omega, T)$ is thus given by

$$\omega_m^r D(\omega, T) = -\frac{1}{2\pi} \text{Im} \sum_{\sigma} \left[(\omega_m^r)^{-1} (\Delta(\omega) - \tilde{\Sigma}_{\sigma}(\omega, T)) \right]^{-1} \quad (5.1)$$

where (from equations (2.3,4)) the hybridization $\Delta(\omega) = \Delta(\tilde{\omega}\omega_m)$ reduces simply to $(\omega_m^r)^{-1} \Delta(\omega) = -\text{sgn}(\omega)[\beta(r) + i]|\tilde{\omega}|^r$ (and, trivially, the bare $\omega = \omega_m \tilde{\omega}$ of equation (2.11) may be neglected). We consider explicitly $\omega \geq 0$ in the following, since $D(-\omega, T) = D(\omega, T)$ from particle-hole symmetry.

Our task now is to demonstrate that $(\omega_m^r)^{-1} \tilde{\Sigma}_{\uparrow}(\omega, T)$ is a function solely of $\tilde{\omega}$ and \tilde{T} in the GFL phase. It follows from equation (4.4) that

$$\Sigma_{\uparrow}^{\text{I}}(\omega, T) = U^2 \int_{-\infty}^{\infty} d\omega_1 \chi^{+-}(\omega_1) D_{\downarrow}^0(\omega_1 + \omega) \quad (5.2)$$

$$\times [\theta(\omega_1) f(\omega_1 + \omega) + \theta(-\omega_1)(1 - f(\omega_1 + \omega))]$$

(with the temperature dependence of $f(\omega, T)$ temporarily omitted). In the requisite strong coupling regime $U \gg 1$, $\chi^{+-}(\omega, T) \simeq \text{Im} \Pi^{+-}(\omega) = \pi \delta(\omega - \omega_m)$ is readily shown to reduce asymptotically to a δ -function centred on $\omega = \omega_m$; and thus $\Sigma_{\uparrow}^{\text{I}}(\omega, T) = \pi U^2 D_{\downarrow}^0(\omega_m[1 + \tilde{\omega}]) f(1 + \tilde{\omega}, \tilde{T})$ (noting that $f(\omega, T)$ depends solely on the ratio ω/T). Using equation (4.3), $D_{\downarrow}^0(\omega) \sim 4|\omega|^r/\pi U^2$ in strong coupling; whence

$$(\omega_m^r)^{-1} \Sigma_{\uparrow}^{\text{I}}(\omega, T) = 4|1 + \tilde{\omega}|^r f(1 + \tilde{\omega}, \tilde{T}) \quad (5.3)$$

which is indeed universally dependent solely on $\tilde{\omega}$ and \tilde{T} . We now consider the real part $\tilde{\Sigma}_{\uparrow}^{\text{R}}(\omega, T)$. For $T = 0$ it is known to be given by³⁹

$$(\omega_m^r)^{-1} \tilde{\Sigma}_{\uparrow}^{\text{R}}(\omega, 0) = -\gamma(r)[|1 + \tilde{\omega}|^r - 1] \quad (5.4)$$

where $\gamma(r) = 4/\sin(\pi r) \sim 4/\pi r$, scaling solely in terms of $\tilde{\omega}$ and correctly satisfying symmetry restoration ($\tilde{\Sigma}_{\uparrow}^{\text{R}}(0, 0) = 0$) for the GFL phase. The finite- T difference $\delta \tilde{\Sigma}_{\uparrow}^{\text{R}}(\omega, T) = \Sigma_{\uparrow}^{\text{R}}(\omega, T) - \Sigma_{\uparrow}^{\text{R}}(\omega, 0)$ is readily calculated via Hilbert transforms using equation (5.2). After some manipulation it is found to be given by

$$(\omega_m^r)^{-1} \delta \tilde{\Sigma}_{\uparrow}^{\text{R}}(\omega, T) = -\frac{4}{\pi} \tilde{T}^r H \left(\frac{|1 + \tilde{\omega}|}{\tilde{T}} \right). \quad (5.5)$$

$H(y)$ is defined as

$$H(y) = \int_0^{\infty} d\omega \frac{\omega^r}{\exp(\omega) + 1} \mathcal{P} \left(\frac{1}{\omega + y} + \frac{1}{\omega - y} \right) \quad (5.6)$$

and is trivial to evaluate numerically; its $y \gg 1$ and $y \ll 1$ asymptotic behaviour is also obtainable in closed form, as used below. From equations (5.4,5), we thus obtain

$$(\omega_m^r)^{-1} \tilde{\Sigma}_{\uparrow}^{\text{R}}(\omega, T) = -\gamma(r)[|1 + \tilde{\omega}|^r - 1] - \frac{4}{\pi} \tilde{T}^r H \left(\frac{|1 + \tilde{\omega}|}{\tilde{T}} \right). \quad (5.7)$$

The complete GFL scaling spectrum now follows from equations (5.1) and (5.3,7); and, as required, $\omega_m^r D(\omega, T)$ is seen to be a universal function of $\tilde{\omega} = \omega/\omega_m$ and $\tilde{T} = T/\omega_m$.

Before proceeding to a comparison with figure 3 however, we add that $\omega_m^r D(\omega, T)$ is equivalently a universal function of $\omega/T \equiv \omega'$ and \tilde{T}^{-1} . To see this note that equations (5.3,7) may be rewritten as

$$(T^r)^{-1} \Sigma_{\uparrow}^{\text{I}}(\omega, T) = 4 \left| \omega' + \frac{1}{\tilde{T}} \right|^r f \left(\frac{1}{\tilde{T}} + \omega' \right) \quad (5.8)$$

and

$$(T^r)^{-1} \tilde{\Sigma}_{\uparrow}^{\text{R}}(\omega, T) = -\gamma(r) \left[\left| \omega' + \frac{1}{\tilde{\omega}} \right|^r - \tilde{T}^{-r} \right] - \frac{4}{\pi} H \left(\left| \omega' + \frac{1}{\tilde{T}} \right| \right) \quad (5.9)$$

(with notation $f(z) \equiv f(z, 1) = [\exp(z) + 1]^{-1}$ for the Fermi functions), which depend solely on ω' and \tilde{T}^{-1} . From equation (5.1) it follows directly that

$$\pi T^r D(\omega, T) = -\frac{1}{2} \text{Im} \sum_{\sigma} \left\{ (T^r)^{-1} \left[\Delta(\omega) - \tilde{\Sigma}_{\sigma}(\omega, T) \right] \right\}^{-1} \quad (5.10)$$

which is thus of form

$$\pi T^r D(\omega, T) \equiv S_{\text{GFL}} \left(\frac{\omega}{\tilde{T}}, \frac{1}{\tilde{T}} \right). \quad (5.11)$$

The importance of this result is that from it the finite- T spectrum *at the QCP itself* (cf equation (3.8)) may be obtained explicitly, since the QCP corresponds to $\omega_m = 0$ i.e. $\tilde{T}^{-1} = 0$. We consider this issue explicitly in section 5.3.

First we compare directly the analytic results above for the GFL phase, with the numerical results given in figure 3. Figure 4 shows the modified spectral function $\mathcal{F}(\omega)$ versus $\tilde{\omega} = \omega/\omega_m$ for $r = 0.2$ arising from equation (5.1,3,7), for the same range of ‘scaled’ temperature $\tilde{T} = T/\omega_m$. The agreement is seen to be excellent: all

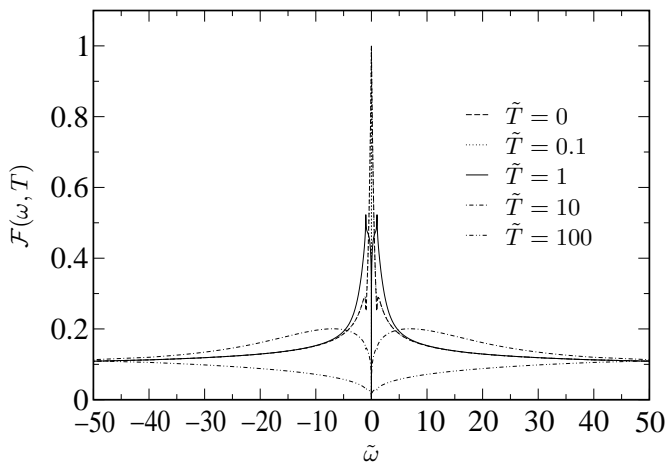


FIG. 4: Analytical results: GFL phase scaling spectrum $\mathcal{F}(\omega, T)$ versus $\tilde{\omega} = \omega/\omega_m$ for $r = 0.2$ and the sequence of temperatures shown.

features of the numerical spectra are captured by the analytical form; quantitative differences are small, and arise because the equations hold asymptotically as $r \rightarrow 0$.

Two specific points concerning the large- $\tilde{\omega}$ behaviour of the GFL phase scaling spectrum may now be made. First, the observation (section 4.1) that for frequencies $|\tilde{\omega}| \gg \tilde{T}$ the scaling spectra are effectively independent of \tilde{T} . For $|\tilde{\omega}| \gg \max(1, \tilde{T})$ the argument of $H(|1 + \tilde{\omega}|/\tilde{T})$ is large and $H(|1 + \tilde{\omega}|/\tilde{T}) \simeq 0$ may be neglected in equation (5.7) ($H(y) \sim -\pi^2/6y^2$ for $y \gg 1$). Hence $(\omega_m^r)^{-1}\tilde{\Sigma}_\uparrow^R(\omega, T) \sim -\gamma(r)[|\tilde{\omega}|^r - 1]$ and $(\omega_m^r)^{-1}\tilde{\Sigma}_\uparrow^I(\omega, T) \sim 4|\tilde{\omega}|^r\theta(-[1 + \tilde{\omega}])$ from equations (5.7,3), and from equation (5.1) it follows that

$$\pi\omega_m^r D(\omega, T) \sim \frac{1}{2|\tilde{\omega}|^r} \left\{ \frac{1}{[\beta(r) + \gamma(r)(1 - |\tilde{\omega}|^{-r})]^2 + 1} + \frac{5}{[\beta(r) - \gamma(r)(1 - |\tilde{\omega}|^{-r})]^2 + 25} \right\} \quad (5.12)$$

The key point here is that equation (5.12) is independent of \tilde{T} , showing explicitly that for $|\tilde{\omega}| \gg \max(1, \tilde{T})$ the scaling spectrum indeed coincides with its $T = 0$ limit³⁹.

Second, equation (5.12) shows that the leading large $\tilde{\omega}$ behaviour ($|\tilde{\omega}|^r \gg 1$) of the GFL scaling spectrum is

$$\pi\omega_m^r D(\omega, T) \sim \frac{1}{2|\tilde{\omega}|^r} \left\{ \frac{1}{[\beta(r) + \gamma(r)]^2 + 1} + \frac{5}{[\beta(r) - \gamma(r)]^2 + 25} \right\} \quad (5.13)$$

– i.e. $\omega_m^r D(\omega, T) \propto |\tilde{\omega}|^{-r}$ which, for small r , is very slowly varying. The onset of this powerlaw behaviour for $|\omega|^r \gg 1$ is readily seen in the inset to figure 3.

Finally, since $\gamma(r) = 4/\sin(\pi r) \sim 4/\pi r$ and $\beta(r) = \tan(\frac{\pi r}{2}) \sim \frac{\pi r}{2}$ for $r \ll 1$, the leading low- r behaviour of

the high-frequency asymptotic ‘tails’ equation (5.13) is

$$\pi\omega_m^r D(\omega, T) \sim \frac{3\pi^2 r^2}{16} |\tilde{\omega}|^{-r} \quad (5.14)$$

precisely as found hitherto for $T = 0$ ³⁹; and since the scale ω_m^r drops out of equation (5.14), the low- ω behaviour of the $T = 0$ QCP spectrum itself (where $\omega_m = 0$) follows immediately as³⁹

$$\pi D(\omega, 0) = \frac{3\pi^2 r^2}{16} |\omega|^{-r} \quad (5.15)$$

which result is believed to be asymptotically exact as $r \rightarrow 0$.

B. LM phase

While the general form equation (5.10) for $T^r D(\omega, T)$ naturally applies to both phases, symmetry is not of course restored for $U > U_c$ in the LM phase^{39,40}: the renormalized level $\tilde{\Sigma}_\uparrow^R(0, 0)$ is non-zero. But it necessarily vanishes as $U \rightarrow U_c+$ and the LM→GFL transition is approached, and in consequence determines a low-energy scale ω_L characteristic of the LM phase as discussed in §3.1. Given explicitly by

$$\omega_L = [|\tilde{\Sigma}_\uparrow^R(0, 0)|/\gamma(r)]^{\frac{1}{r}} \quad (5.16)$$

this is the natural scaling counterpart to ω_m in the GFL phase, such that the $T = 0$ LM phase spectrum scales universally as a function of $\tilde{\omega} = \omega/\omega_L$ ^{39,40}.

The required results for $\tilde{\Sigma}_\uparrow(\omega, T)$ in the LM phase are obtained most directly from their counterpart equations (5.8,9) in the GFL phase (in which $1/\tilde{T} = \omega_m/T$ and $1/\tilde{\omega} = \omega_m/\omega$), by setting $\omega_m = 0$ therein — recall that the spin-flip scale vanishes identically throughout the LM phase, where $\chi^{+-}(\omega, T) \simeq \text{Im}\Pi^{+-}(\omega) = \pi\delta(\omega)$. Equation (5.8) then yields

$$(T^r)^{-1}\tilde{\Sigma}_\uparrow^I(\omega, T) = 4|\omega'|^r f(\omega'). \quad (5.17)$$

$T^{-r}[\tilde{\Sigma}_\uparrow^R(\omega, T) - \tilde{\Sigma}_\uparrow^R(0, 0)]$ is likewise obtained by setting $\omega_m = 0$ in the right side of equation (5.9). Using equation (5.16) for $\tilde{\Sigma}_\uparrow^R(0, 0) = -|\tilde{\Sigma}_\uparrow^R(0, 0)|$, this gives

$$(T^r)^{-1}\tilde{\Sigma}_\uparrow^R(\omega, T) = -\gamma(r)[\tilde{T}^{-r} + |\omega'|^r] - \frac{4}{\pi}H(\omega') \quad (5.18)$$

in which $\tilde{T} = T/\omega_L$ (and $\omega' = \omega/T \equiv \tilde{\omega}/\tilde{T}$).

Equations (5.17,18) and (5.10) generate the LM phase scaling spectrum. It is thus seen to be of form

$$\pi T^r D(\omega, T) = S_{\text{LM}} \left(\frac{\omega}{\tilde{T}}, \frac{1}{\tilde{T}} \right) \quad (5.19)$$

scaling universally in terms of ω' and \tilde{T} ; or, entirely equivalently, that $\omega_m^r D(\omega, T)$ scales in terms of $\tilde{\omega} = \omega/\omega_L$

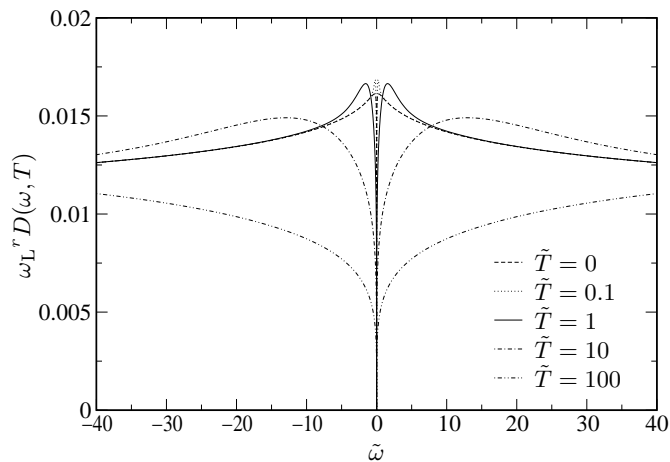


FIG. 5: LM phase scaling spectrum $\omega_L^r D(\omega, T)$ versus $\tilde{\omega} = \omega/\omega_L$ for $r = 0.2$ and a sequence of temperatures $\tilde{T} = T/\omega_L$.

and \tilde{T} . The scaling spectra so obtained are shown in figure 5 for a range of \tilde{T} . It is again readily shown that for $|\tilde{\omega}| \gg \tilde{T}$ the LM phase scaling spectra are effectively independent of \tilde{T} and coincide with the $\tilde{T} = 0$ limit³⁹, and from which the low- ω behaviour of the $T = 0$ QCP spectrum (equation (5.15)) correctly follows by taking $\omega_L \rightarrow 0$.

C. Quantum critical point

We turn now to the quantum critical point itself. It has been shown in §3 that the QCP spectrum must exhibit pure $\omega' = \omega/T$ scaling, *ie* that $\pi T^r D(\omega, T) = S(\omega')$. In §s 5.1,2 we have also shown that this general behaviour is correctly recovered by the local moment approach (which is distinctly non-trivial, bearing in mind that the QCP is an interacting, non-Fermi liquid fixed point). Our aims now are twofold. First to obtain explicitly the scaling function $S(\omega')$ arising within the LMA for $r \ll 1$; and then to show that it is uniformly recovered from GFL/LM scaling spectrum as $\tilde{T} = T/\omega_* \rightarrow \infty$ (we remind the reader that $\omega_* \equiv \omega_m$ in the GFL phase and $\omega_* \equiv \omega_L$ for the LM phase).

Taking $\tilde{T}^{-1} = 0$ in equations (5.17,18) (or equations (5.8,9)) gives

$$(T^r)^{-1} \Sigma_{\uparrow}^I(\omega, T) = 4|\omega'|^r f(\omega') \quad (5.20)$$

$$(T^r)^{-1} \tilde{\Sigma}_{\uparrow}^R(\omega, T) = -\gamma(r)|\omega'|^r - \frac{4}{\pi} H(\omega'). \quad (5.21)$$

The QCP scaling spectrum $\pi T^r D(\omega, T) \equiv S(\omega')$ now follows directly from equation (5.10).

Figure 6 shows the resultant QCP spectrum for $r = 0.2$, as a function of $\omega' = \omega/T$ on a logarithmic scale.

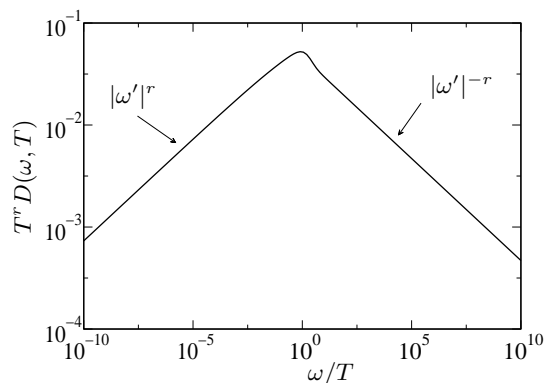


FIG. 6: QCP scaling spectrum $T^r D(\omega, T)$ versus $\omega' = \omega/T$ for $r = 0.2$. $\omega' \simeq 1$ marks a crossover from $|\omega'|^{-r}$ behaviour for $|\omega'| \gg 1$ to $|\omega'|^r$ behaviour for $|\omega'| \ll 1$.

From this it is clear that two distinct power law behaviours dominate. For $|\omega'| \ll 1$, where $H(\omega') \sim r^{-1}(1 - |\omega'|^r) + c$ (with $c = \ln(\frac{\pi}{2}\exp(-C)) \simeq -0.125$ a constant, and C Euler's constant), it follows that

$$\pi T^r D(\omega, T) \underset{|\omega'| \ll 1}{\sim} \frac{3\pi^2 r^2}{16} |\omega'|^r. \quad (5.22)$$

This behaviour is clearly seen in the figure 6, and in practice sets in for $|\omega'| \lesssim 1$.

For $|\omega'| \gg 1$ by contrast, where $H(\omega') \simeq 0$ may be neglected, equations (5.10,20,21) give

$$\pi T^r D(\omega, T) \underset{|\omega'| \gg 1}{\sim} \frac{3\pi^2 r^2}{16} |\omega'|^{-r}. \quad (5.23)$$

This form is also clearly evident in figure 6, in practice setting in above $|\omega'| \gtrsim 1$. Such behaviour is also precisely the general form deduced in section 3 (equation (3.9)) on the assumption that the limits $\omega_* \rightarrow 0$ and $T \rightarrow 0$ commute; with the explicit r -dependence $C(r) = 3\pi^2 r^2/16$, which we believe to be asymptotically exact as $r \rightarrow 0$, obtainable because the result now arises from a microscopic many-body theory.

As discussed in section 3 and above, the GFL/LM scaling spectra may be expressed as functions of $\omega' = \omega/T$ for any given \tilde{T} . One obvious question then arises: how do the GFL/LM scaling spectra evolve with temperature \tilde{T} to approach their ultimate limit of the QCP spectrum as $\tilde{T} \rightarrow \infty$? This is illustrated in figure 7 where the analytic results of sections 5.1 and 5.2 are replotted versus $\omega' = \omega/T$ for a sequence of increasing temperatures $\tilde{T} = T/\omega_*$. The QCP scaling spectrum is shown as a thick dashed line. From figure 7 we see that — for all \tilde{T} — the GFL and LM scaling spectra coincide both with each other and with the QCP scaling spectrum for $|\omega'| \gg 1$. This is a reflection of two facts. First, as discussed in sections 5.1 and 5.2, that the high-frequency behaviour of the GFL and LM phase spectra coincide with their $\tilde{T} = 0$ limits. And second, that the high-frequency tails

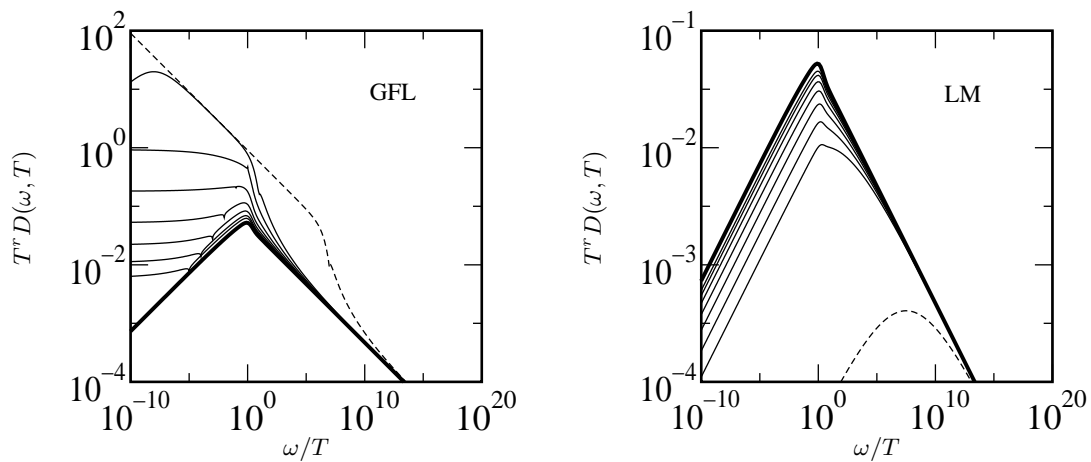


FIG. 7: The left (right) panel shows the GFL (LM) phase scaling spectrum $T^r D(\omega, T) \equiv S_{\text{GFL}}(\omega', \tilde{T}^{-1})$ versus $\omega' = \omega/T$ for $\tilde{T} = 10^{-1}, 10^0, 10^1, 10^2, 10^3, 10^4, 10^5$ and ∞ (in sequence top→bottom for the GFL phase and bottom→top for LM). In either case the QCP spectrum $\tilde{T} = \infty$ is shown as a thick line; the dotted line shows the $\tilde{T} \rightarrow 0$ spectrum.

of the $T = 0$ GFL/LM scaling spectrum coincide with those of the $T = 0$ QCP spectrum.

Most importantly, however, figure 7 shows that the QCP scaling spectrum is obtained ‘uniformly’ from the GFL/LM phase scaling spectrum upon increasing temperature \tilde{T} . That is, with progressively increasing \tilde{T} the GFL/LM phase scaling spectra ever increasingly coincide with the QCP scaling spectrum (thick line) over a larger and larger frequency interval, such that in the limit $\tilde{T} \rightarrow \infty$ the QCP spectrum for all ω/T is obtained smoothly. This is an important result, providing as it does a direct connection between the QCP scaling spectrum and scaling spectra in the GFL or LM phases at any finite \tilde{T} .

VI. SUMMARY

We have considered a local moment approach to the pseudogap Anderson impurity model, close to the symmetric quantum critical point where the Kondo resonance has just collapsed. Building on previous work^{39,40,48}, we have focused on single-particle dynamics at finite

temperature, obtaining an analytical description of the finite- T scaling behaviour for small r , in both generalized Fermi liquid (Kondo screened) and local moment phases. A key result obtained on general grounds is that pure ω/T -scaling obtains at the QCP itself, consistent with an interacting fixed point and recent results for the local dynamical susceptibility³⁶. We have succeeded both in obtaining explicitly the QCP scaling spectrum, and in understanding its continuous emergence with increasing T/ω_* from the scaling dynamics appropriate to the Kondo screened and local moment phases on either side of the quantum phase transition.

Related results have also been obtained for the PAIM with finite local magnetic field, $h = g\mu_B H_{\text{loc}}$ ^{49,50}; i.e. pure ω/h -scaling of the single-particle spectrum at the QCP. These will be discussed elsewhere.

Acknowledgements

The authors would like to express their appreciation to the EPSRC, Leverhulme Trust and Balliol College Oxford for support; and to Kevin Ingersent for helpful discussions regarding the present work.

* Current address: Department of Physics, University of Florida, Gainesville, Florida 32611-8440, USA.

† Electronic address: dlogan@physchem.ox.ac.uk

¹ Stewart G R 2001 *Rev. Mod. Phys.* **73** 797

² Coleman P *et al* 2001 *J. Phys.: Condens. Matter* **13** R723; Coleman P 1999 *Physica B* **261** 353

³ v. Löhneyson H *et al* (1994) *Phys. Rev. Lett.* **72** 3262

⁴ Heuser K *et al* 1998 *Phys. Rev. B* **57** R4198

⁵ Küchler R *et al* 2004 *cond-mat/0407798*

⁶ Mathur N D *et al* 1998 *Nature* **394** 39

⁷ Trovarelli O *et al* 2000 *Phys. Rev. Lett.* **85** 626

⁸ Schröder A *et al* 2000 *Nature* **407** 351; 1998 *Phys. Rev. Lett.* **80** 5623

⁹ Stockert O *et al* 1998 *Phys. Rev. Lett.* **80** 5627

¹⁰ Hertz J A 1976 *Phys. Rev. B* **14** 1165

¹¹ Millis A J 1993 *Phys. Rev. B* **48** 7183

¹² Moriya T and Takimoto T 1995 *J. Phys. Soc. Jpn.* **64** 960

¹³ Si Q., Rabello S., Ingersent K. and Smith J. L. 2001 *Nature* **413** 804

¹⁴ Smith J L and Si Q 1999 *Europhys. Lett.* **45** 228

¹⁵ Zhu L and Si Q 2002 *Phys. Rev. B* **66** 024426

¹⁶ Grempel D R and Si Q 2003 *Phys. Rev. Lett.* **91** 026401

- ¹⁷ Zhu L *et al* 2003 Phys. Rev. Lett. **91** 156404
- ¹⁸ Burdin S *et al* 2003 Phys. Rev. B **67** 121104
- ¹⁹ Withoff D and Fradkin E 1990 Phys. Rev. Lett. **64** 1835
- ²⁰ Anderson P W 1961 *Phys. Rev.* **124** 41
- ²¹ Hewson A C 1993 *The Kondo Problem to Heavy Fermions* (Cambridge: Cambridge University Press)
- ²² Gehring G A 2002 *J. Phys.: Condens. Matter* **14** V5
- ²³ Kouwenhoven L and Glazman L 2001 (January) *Physics World* 33
- ²⁴ Cronenwett *et al* 1998 *Science* **281** 540
- ²⁵ Volkov B A and Pankratov O A 1985 *Pis. Zh. Eksp. Teor. Fiz.* **42** 145
(ENGL. TRANSL. 1985 *JETP Lett.* **42** 178)
- ²⁶ Voit J 1995 Rep. Prog. Phys. **58** 977
- ²⁷ Vojta M 2001 Phys. Rev. Lett. **87** 097202
- ²⁸ Vojta M and Bulla R 2002 Phys. Rev. B **65** 014511
- ²⁹ Hopkinson J *et al* (2004) cond-mat/0407583
- ³⁰ Ingersent K 1996 Phys. Rev. B **54** 11936
- ³¹ Gonzalez-Buxton C and Ingersent K 1996 Phys. Rev. B **54** 15614
- ³² Chen K and Jayaprakash C 1995 *J. Phys.: Condens. Matter* **7** L491
- ³³ Bulla R, Pruschke Th and Hewson A C 1997 *J. Phys.: Condens. Matter* **9** 10463
- ³⁴ Gonzalez-Buxton C and Ingersent K 1998 Phys. Rev. B **57** 14254
- ³⁵ Bulla R, Glossop M T, Logan D E and Pruschke T 2000 *J. Phys.: Condens. Matter* **12** 4899
- ³⁶ Ingersent K. and Si Q. 2002 Phys. Rev. Lett. **89** 076403
- ³⁷ Fritz L and Vojta M 2004 cond-mat/0408543
- ³⁸ Logan D E and Glossop M T 2000 *J. Phys.: Condens. Matter* **12** 985
- ³⁹ Glossop M T and Logan D E 2003 *Europhys. Lett.* **61** 810
- ⁴⁰ Glossop M T and Logan D E 2003 *J. Phys.: Condens. Matter* **15** 7519
- ⁴¹ Cassanello C R and Fradkin E 1996 Phys. Rev. B **53** 15079
- ⁴² Ingersent K and Si Q 1998 cond-mat/9810226
- ⁴³ Borkowski L S 1997 Acta Physica Polonica A **91** 359
- ⁴⁴ Glossop M T and Logan D E 2000 *Eur. Phys. J. B* **13** 513
- ⁴⁵ Logan D E, Eastwood M P and Tusch M A 1998 *J. Phys.: Condens. Matter* **10** 2673
- ⁴⁶ Dickens N L and Logan D E 2001 *J. Phys.: Condens. Matter* **13** 4505
- ⁴⁷ Glossop M T and Logan D E 2002 *J. Phys.: Condens. Matter* **14** 6737
- ⁴⁸ Logan D E and Dickens N L 2002 *J. Phys.: Condens. Matter* **14** 3605
- ⁴⁹ Logan D E and Dickens N L 2001 *Europhys. Lett.* **54** 227
- ⁵⁰ Logan D E and Dickens N L 2001 *J. Phys.: Condens. Matter* **13** 9713
- ⁵¹ Vidhyadhiraja N S, Smith V E, Logan D E and Krishnamurthy H R 2003 *J. Phys.: Condens. Matter* **15** 4045
- ⁵² Smith V E, Logan D E and Krishnamurthy H R 2003 *Eur. Phys. J. B* **32** 49
- ⁵³ Vidhyadhiraja N S and Logan D E 2004 *Eur. Phys. J. B* **39** 313